5-19-2012

A Field Proof-of-Concept of Aquifer Imaging Using 3-D Transient Hydraulic Tomography with Modular, Temporarily-Emplaced Equipment

Michael Cardiff
Boise State University

Warren Barrash
Boise State University

Peter K. Kitanidis
Stanford University

 DOI: 10.1029/2011wr011704

A field proof-of-concept of aquifer imaging using 3-D transient hydraulic tomography with modular, temporarily-emplaced equipment

M. Cardiff,[1,2] W. Barrash,[1] and P. K. Kitanidis[3]

Received 1 December 2011; revised 13 March 2012; accepted 30 March 2012; published 19 May 2012.

[1] Hydraulic tomography is a field scale aquifer characterization method capable of estimating 3-D heterogeneous parameter distributions, and is directly sensitive to hydraulic conductivity (K), thus providing a useful data source for improving flow and transport models. We present results from a proof-of-concept field and modeling study in which we apply 3-D transient hydraulic tomography (3DTHT) to the relatively high-K and moderately heterogeneous unconfined aquifer at the Boise Hydrogeophysical Research Site. Short-duration (20 min) partially penetrating pumping tests, for which observed responses do not reach steady state, are used as the aquifer stimulation. To collect field data, we utilize a system of temporarily emplaced packer equipment to isolate multiple discrete intervals in boreholes. To analyze the data, we utilize MODFLOW combined with geostatistical inversion code based on the quasilinear approach of Kitanidis (1995). This combination of practical software allows inversion of large datasets (>250 drawdown curves, and almost 1000 individual data points) and estimation of K at >100,000 locations; reasonable runtimes are obtained using a single multicore computer with 12 GB of RAM. The K heterogeneity results from 3DTHT are cross-validated against K characterization from a large set of partially penetrating slug tests, and found to be quite consistent. The use of portable, modular equipment for field implementation means that 3DTHT data collection can be performed (including mobilization/demobilization) within a matter of days. Likewise, use of a practical, efficient and scalable numerical modeling and inversion strategy means that computational effort is drastically reduced, such that 3-D aquifer property distributions can be estimated quickly.

Citation: Cardiff, M., W. Barrash, and P. K. Kitanidis (2012), A field proof-of-concept of aquifer imaging using 3-D transient hydraulic tomography with modular, temporarily-emplaced equipment, *Water Resour. Res.*, *48*, W05531, doi:10.1029/2011WR011704.

1. Introduction

[2] Hydraulic conductivity (K), the key parameter which controls groundwater flow and solute movement in the subsurface, is variable throughout the subsurface over a wide range in magnitudes (10^{-12} m s^{-1} for tight clays to 10^{-1} m s^{-1} for coarse gravels) and varies at many different spatial scales, from less than m^3 to greater than km^3. Knowledge of this variability is often key to making good predictions about future aquifer behavior and to improving decision making in aquifer management and remediation scenarios. For example, even at the small scale of DNAPL source zones (100 m^3 – 10,000 m^3), heterogeneity in hydraulic conductivity of as little as $1-2$ orders of magnitude has been shown to highly influence source zone architecture (i.e., the development of structures such as pools, lenses, ganglia, and residual DNAPL) and hence control, in part, the development and evolution of associated dissolved-phase contaminant plumes as well as the effectiveness of DNAPL remediation strategies [e.g., *Dekker and Abriola*, 2000; *Conrad et al.*, 2002; *Page et al.*, 2007].

[3] A large body of research in subsurface hydrology is concerned with the attainment of the spatial distribution of K as well as other subsurface parameters (e.g., porosity θ, specific storage S_s, dispersivities, and specific yield S_y). Focusing on characterization strategies that have been applied in the field and analyzed for aquifer heterogeneity characterization, research in estimating subsurface flow parameter heterogeneity is broadly divisible into five main categories: (1) Sample-based methods; (2) Pressure-based methods; (3) Tracer-based methods; (4) Geophysical methods; and (5) Combination methods. We define sample-based methods as those for which a section of aquifer material at known location/depth is recovered from the subsurface and analyzed (for composition, flow properties, or geophysical behavior); this is the one characterization method that is carried out ex situ. Pressure-based methods are those for

[1]Department of Geosciences, Boise State University, Boise, Idaho, USA.
[2]Department of Geoscience, University of Wisconsin-Madison, Madison, Wisconsin, USA.
[3]Department of Civil and Environmental Engineering, Stanford University, Stanford, California, USA.

0043-1397/12/2011WR011704

which changes in water pressure associated with aquifer stimulations are the primary source of measurements. This category includes methods that use human-induced stimulations—such as fully penetrating pumping tests [*Vasco et al.*, 2000; *Straface et al.*, 2007; *Li et al.*, 2007; *Vasco*, 2008; *Cardiff et al.*, 2009; *Huang et al.*, 2011], partially penetrating pumping tests (*Vasco and Karasaki* [2001, 2006]; *Bohling et al.* [2007]; *Bohling* [2009]; *Illman et al.* [2009], and the current work), slug tests [*Springer and Gelhar*, 1991; *Butler*, 2002; *Alexander et al.*, 2010; *Brauchler et al.*, 2010, 2011; *Cardiff et al.*, 2011], borehole flowmeters [e.g., *Hess et al.*, 1992; *Genereux and Guardiario*, 2001; *Williams and Paillet*, 2002; *Fienen et al.*, 2004], and direct-push hydraulic tests [*Cho et al.*, 2000; *Butler et al.*, 2002, 2007; *Dietrich et al.*, 2008]—as well as those that rely on natural stimulations—including river stage fluctuations, and atmospheric (barometric) pressure variations (as proposed by *Yeh et al.* [2009]). Tracer-based methods are those where the primary source of information is the concentration or occurrence of one or more species within an aquifer. As before, the measurements may be the result of human-induced stimulations—an injected conservative or nonconservative solute, colloid, or immiscible liquid [e.g., *Roberts et al.*, 1986; *Curtis et al.*, 1986; *Sudicky*, 1986; *Freyberg*, 1986; *Mackay et al.*, 1986; *Harvey et al.*, 1989; *LeBlanc et al.*, 1991; *Garabedian et al.*, 1991; *Ptak and Schmid*, 1996; *Bohling*, 1999; *Sutton et al.*, 2000; *Jawitz et al.*, 2003]—or may be associated with naturally occurring or preexisting tracers—e.g., isotopes, salinity, temperature, or soluble compounds [e.g., *Solomon et al.*, 1992; *Weissmann et al.*, 2002; *Cook et al.*, 2005]. Geophysical methods represent somewhat of a catchall term where the primary measurements used are neither water pressure nor tracer measurements—this includes a broad array of techniques such as those that rely on electrical [e.g., *Watson et al.*, 2005; *Slater*, 2007; *Crook et al.*, 2008; *Nyquist et al.*, 2008; *Clifford and Binley*, 2010], electromagnetic [e.g., *Beres et al.*, 1995; *Asprion and Aigner*, 1999; *Tronicke et al.*, 2004; *Bradford et al.*, 2009; *Bayer et al.*, 2011], or seismic [e.g., *Ellefsen et al.*, 2002; *Daley et al.*, 2004; *Moret et al.*, 2006] stimulations, or combinations of multiple geophysical stimulations [e.g., *Linde et al.*, 2006, 2008; *Doetsch et al.*, 2010a, 2010b]. Lastly, combination methods use combinations of measurements and/or stimulations from the previous three categories [e.g., *Hyndman and Gorelick*, 1996; *Slater et al.*, 2000; *Kemna et al.*, 2002; *Singha and Gorelick*, 2005; *Day-Lewis et al.*, 2006; *Hubbard et al.*, 2008; *Dafflon et al.*, 2011b; *Straface et al.*, 2011].

[4] Pressure-based methods have both advantages and disadvantages relative to other methods. Advantages of pressure-based methods as a flow parameter estimation strategy are that: (1) they are sensitive to flow parameter variability in areas that are not disturbed by drilling, in contrast to sample-based methods; (2) they are directly sensitive to flow parameter variability, in contrast to strictly geophysical methods; and (3) in general, they are less time, labor, and equipment intensive to perform than tracer-based methods or combination methods, and likewise they are often simpler to model and analyze than tracer or combination methods. Relative to the other methods available, though, pressure-based methods are generally more time consuming than geophysical methods for characterizing comparable scales. In addition, in some cases pressure-based methods may not provide sufficient information to accurately image heterogeneity at a scale that predicts macrodispersive properties important in contaminant transport; in cases where such predictions are crucial, longer-duration tracer tests may provide additional predictive capabilities beyond pressure-based methods. However, it is important to note that any tracer test must be designed such that the tracer plume encounters the heterogeneous features of interest; very little information about heterogeneity is expected in areas of a site that a tracer test plume does not pass through.

[5] Within the particular realm of pressure-based methods, there is a large variety of physical tools that can be combined in various ways in order to perform imaging of 3-D (saturated zone) flow parameter heterogeneity. All pressure-based methods require access to the saturated zone, with the two most favored methods being well drilling and direct push. In direct push investigations, the direct push permeameter may be used to provide both a stimulation (injection of water) and a measurement of response (pressure changes) at two nearly colocated points [*Butler et al.*, 2007], which is used to characterize the effective flow parameters at a given point as the tool is advanced through the aquifer depth. Slug testing strategies for direct push setups may also be used to obtain local parameter estimates as a tool is advanced [e.g., *Butler*, 2002]. Alternately, a screened interval can be installed at the end of a direct push rod and used solely as a pressure measurement point, with the stimulation taking place via pumping at another location [e.g., *Butler et al.*, 2002; *Dietrich and Leven*, 2009]. In drilled wells, a variety of methods may also be used to obtain 3-D information. Partially penetrating slug test equipment can be used to isolate a given depth interval in a well (using a set of inflatable packers) and then perform both stimulation and pressure observations at the same location [*Bouwer and Rice*, 1976; *Zlotnik and McGuire*, 1998; *Butler*, 1998; *Cardiff et al.*, 2011]. Other equipment for obtaining vertical variability in K near a fully penetrating well (using pressure signals) include dipole flow cell apparati [e.g., *Kabala*, 1993; *Zlotnik and Zurbuchen*, 1998] and borehole flow meters [e.g., *Paillet*, 1998; *Hess*, 1986; *Hess*, 1989; *Molz et al.*, 1994]. Alternately, a single fully penetrating borehole can be segmented into multiple observation zones using either permanent apparati that are installed at the time of well drilling (e.g., continuous multichannel tubing (CMT), *Einarson and Cherry* [2002])—or by using temporary packer and port strings that can be placed down well and inflated to isolate given depth locations and removed after usage (e.g., the Waterloo system, *Pianosi and Belshaw* [1990]). Once installed, this hardware can be used to take depth-dependent pressure measurements during aquifer stimulation by, e.g., pumping tests or slug tests performed at other wells.

[6] Similarly, in addition to the broad range of physical tools available to investigators for pressure-based flow parameter characterization, there are also a number of analysis methodologies that can be employed after collecting data. In the most basic case, analytical solutions assuming homogeneous flow parameter values in the "region of influence" of a test can be developed (i.e., analytical methods), and

field data can be fit to these solutions resulting in an "effective" K value for the region investigated. Generally for analytical methods multiple aquifer tests are analyzed separately, with effective K values assigned to the different regions influenced by each test, resulting in an approximate image of aquifer heterogeneity. While computationally convenient, effective parameters obtained assuming homogeneity result from an averaging of local heterogeneities near the testing location that may be poorly understood [*Wu et al.*, 2005; *Beckie and Harvey*, 2002]. At the other end of the spectrum, tomographic methods use numerical models to explicitly represent complex subsurface heterogeneity. In tomographic methods, data from numerous available tests are fit at the same time by algorithmically altering the heterogeneity contained in the numerical model, and an image (or multiple images) of subsurface heterogeneity is developed that is consistent with the full set of observations.

[7] The analysis of pressure-based signals from a series of tests using tomographic methods has been termed hydraulic tomography (HT). While given a single name, the broad umbrella of HT encompasses many different stimulation types and analysis strategies—a thorough review of this variability in HT applications over the past 15 years is presented in the work of *Cardiff and Barrash* [2011]. Because they require a numerical model to accurately represent aquifer heterogeneity, HT methods generally need larger sets of instrumentation for data collection in addition to a much higher computational demand. However, the additional computational and field effort has been shown to yield details of K heterogeneity between boreholes that is not achievable by other methods (e.g., laboratory and numerical studies include *Liu et al.* [2007], *Zhu and Yeh* [2005], and *Cardiff and Barrash* [2011], respectively)

[8] The objective of the work performed for this paper has been, broadly, to improve the value proposition of HT by using hardware and software tools that reduce the field and computational effort of the technique. In this paper, using available field technology, we describe implementation of a proof-of-concept HT testing regime over the period of a week in a real field-scale aquifer at the Boise Hydrogeophysical Research Site (BHRS) using a modular, portable hardware system that can be applied at other sites. We then apply the computational methodology proposed in the work of *Cardiff and Barrash* [2011], to invert for heterogeneous parameter fields of >100,000 unknowns (i.e., K in each grid block of a numerical model) using only modest computational resources. Due to the highly studied nature of the BHRS, the results can be compared against prior results from other characterization approaches, such as slug testing [*Cardiff et al.*, 2011].

2. Experimental Setup and Operation

[9] The data analyzed in this paper were collected during a week long hydraulic tomography field campaign in August 2010 at the BHRS. During this campaign, a series of short (20 min) single-well pumping tests were performed from progressive isolated depth intervals in each of two different wells, and the pressure changes were monitored at numerous isolated depths in 3 or 4 surrounding wells (depending on the test, see Table 1). We first briefly introduce the field site and then discuss specifics of the data collection.

Table 1. Pumping Test Field Data Inverted

Test Name	Pumping Well	Pumping Interval Location (center, m AMSL)
2 Aug 2011 Test 3[a]	B4	834.7
3 Aug 2011 Test 5[a]	B4	838.6
3 Aug 2011 Test 9[a]	B4	841.6
4 Aug 2011 Test 2[a]	B4	843.6
5 Aug 2011 Test 1	B5	833.7
5 Aug 2011 Test 2	B5	834.7
5 Aug 2011 Test 3	B5	835.7
5 Aug 2011 Test 4	B5	836.6
5 Aug 2011 Test 6	B5	837.6
5 Aug 2011 Test 7	B5	838.6
6 Aug 2011 Test 3	B5	840.6
6 Aug 2011 Test 7	B5	844.6

[a]Problems prevented inflation of packer in well B2, data for B2 not inverted.

2.1. Field Site

2.1.1. Site Description

[10] The hydrogeologic setting for this study is the shallow unconfined aquifer at the BHRS, consisting of ≈20 m of mixed sand/gravel/cobble fluvial deposits overlying a clay confining unit. The BHRS is an uncontaminated research well field [*Barrash et al.*, 1999] located on a gravel bar adjacent to the Boise River and roughly 15 km southeast from downtown Boise, Idaho USA (Figure 1). A primary objective for the BHRS has been to determine 3-D distributions of geologic, geophysical, and hydrologic (K, θ, S_s, and S_y) parameters from testing at a variety of scales and dimensionalities. This information provides the basis for (1) developing methods for jointly inverting and interpreting geophysical and hydrologic data (hydrogeophysics) to improve groundwater remediation and other engineering applications with minimally invasive, quantitative, site characterization methods, and (2) more general research opportunities on theory, modeling, and methods using a field-scale "known" control volume in a generic type of heterogeneous aquifer [*National Research Council*, 2000a, 2000b].

[11] In the aquifer, 18 wells were cored through the unconsolidated, cobble and sand fluvial deposits and completed into the underlying clay during 1997–1998. All wells are 10 cm ID PVC and are fully screened through the fluvial aquifer. The wells were advanced with the core-drill-drive method to minimize the disturbed volume of formation outside the wells [*Morin et al.*, 1988; *Barrash et al.*, 2006]; with this method the formation was allowed to collapse against the slotted casing upon withdrawal of the drive casing and no gravel pack was installed. Of the 18 wells, 13 wells are concentrated in the 20 m diameter central area of the BHRS (the A, B and C wells in Figure 1), and five are "boundary" wells (the X wells in Figure 1). The 13 wells in the central area are arranged in two concentric rings (the B and C wells) around a central well (A1).

[12] Natural hydrologic flow at the site is primarily affected by both daily evapotranspiration cycles and river-stage changes, though the latter are only significant during upstream dam operational changes. Due to the short timeframe over which the 3DTHT tests were run (≈20 min per test), and the

Figure 1. Map showing location of BHRS relative to Boise River. Inset shows geometric layout of wells in the central area of the site. Diversion Dam, which controls river levels, can be seen in lower right.

fact that dam operational changes did not occur during testing, the effects of both of these secular influences on measured pressure responses is minimal.

2.1.2. Prior Characterization Results

[13] Stratigraphy initially recognized through neutron porosity logs [*Barrash and Clemo*, 2002] and core analysis [*Barrash and Reboulet*, 2004] includes four cobble-dominated units (denoted Units 1–4, with unit numbers following depositional sequence from lower to higher), which are overlain by a sand channel (Unit 5) that thickens toward the Boise River and pinches out in the center of the well field, near well A1. These coarse sediments of the aquifer are underlain by a red clay everywhere at the well field, and by a thin (≈1 m thick) edge of a basalt flow that occurs between the clay and the coarse sediments in portions of the site. As recognized through neutron-based porosity estimates, Units 1 and 3 have relatively low average porosity and low porosity variance, whereas Units 2 and 4 have higher average porosities and more variable porosity; Unit 5 is markedly different from all other units in being a channel sand deposit with only minor gravel, and thus is the highest porosity material [*Barrash and Clemo*, 2002].

[14] Surveys using ground-penetrating radar (GPR) [*Clement and Knoll*, 2006; *Clement et al.*, 2006; *Clement and Barrash*, 2006; *Ernst et al.*, 2007; *Irving et al.*, 2007; *Dafflon et al.*, 2011a], seismic [*Moret et al.*, 2004, 2006], induced polarization [*Slater et al.*, 2011] and capacitive conductivity [*Mwenifumbo et al.*, 2009] methods recognize similar unit structures, suggesting that geophysical survey responses are largely consistent with observed porosity. However, Unit 2 has been further subdivided into two subunits (Unit 2a and 2b) based on differing electrical responses [*Mwenifumbo et al.*, 2009] and GPR responses [*Irving et al.*, 2007; *Ernst et al.*, 2007; *Dafflon et al.*, 2011a]. In addition, patches and lenses within individual stratigraphic layers (e.g., Unit 4) indicate multiscale heterogeneity beyond the larger-scale unit delineations.

[15] Prior investigations of hydraulic conductivity variability throughout the site have been carried out with a variety of methods, including analytical curve fitting of individual fully penetrating pumping tests [*Barrash et al.*, 2006], joint analysis of tracer test breakthrough curves [*Dafflon et al.*, 2011b], tomographic analyses of fully penetrating pumping tests [*Cardiff et al.*, 2009; *Straface et al.*, 2011], analytical curve fitting of evapotranspiration responses in wells [*Malama and Johnson*, 2010], and analytical curve fitting of individual partially penetrating slug test responses [*Cardiff et al.*, 2011]. Each of these methods returns consistent estimates of hydraulic conductivity (see Table 2), with an average magnitude around $4e-4\,\mathrm{m\,s^{-1}}$, and $1-2$ orders of magnitude in K heterogeneity.

2.2. The 2010 HT Field Campaign

[16] During the summer of 2010, a proof-of-concept field campaign at the BHRS was conducted to (1) acquire sufficient high-quality test data to generate 3DTHT quantitative imaging results with uncertainties and (2) identify areas for improvements for field equipment, data acquisition, and forward and inverse modeling, in order to advance the method and work toward a portable, practically implementable HT imaging system.

[17] We designed the 3DTHT experiments as a series of short-duration pumping tests in successive isolated 1 m intervals from each of two pumping wells (B4 and B5), with observations at seven isolated 1 m intervals (with 1 m packers around the intervals) in each of four observation wells (B1, B2, C3, C4) surrounding the pumping wells. Tests were designed for $15-20$ min with a pumping flowrate of at least $0.3\,\mathrm{L\,s^{-1}}$. Recovery periods of ≈30 min were allocated between tests during which the pumping interval was repositioned up 1 m to the next testing interval. Based

Table 2. Peer-Reviewed Studies of BHRS Aquifer in Which K Was Estimated[a]

Testing Years	Test Stimulation(s) Analyzed	Primary Observations Analyzed	Analysis Method	Parameters Estimated	Aquifer Values Obtained ($m\ s^{-1}$)			References
					Min	Average	Max	
1998–1999	18 fully penetrating pumping tests (2-D). Flow Rate Range: 60–120 L/min.	Drawdown curves at 3–5 fully penetrating observation wells per test	Transient responses separately analyzed with homogeneous, unconfined aquifer analytical model with wellbore skin, anisotropy	Effective aquifer K (radial) Effective aquifer K (vertical)	5.00E-04 4.50E-04	7.60E-04 7.10E-04	1.30E-03 1.05E-03	*Barrash et al.* [2006]
2001	Partially penetrating (4 m) tracer injection. Natural gradient flow with minor pumping.	Transient concentration measurements at 20 partially penetrating (0.25 m) intervals in well along path of plume	Transient responses jointly analyzed with numerical modeling of unconfined, heterogeneous K/porosity aquifer (MODFLOW, SEAWAT)	Spatially distributed K	1.00E-04	4.00E-04	8.00E-04	*Dafflon et al.* [2011b][b]
2007	10 fully penetrating dipole pumping tests. Flow Rate Range: 100–260 L/min.	Steady-state drawdown at 15 fully penetrating observation wells per test	Steady-state responses jointly analyzed with heterogeneous unconfined 2-D map-view numerical model (COMSOL)	Spatially distributed thickness-averaged K	6.30E-05	6.30E-04	1.40E-03	*Cardiff et al.* [2009]
2007	1 fully penetrating dipole pumping test. Flow Rate: 260 L/min.	Steady-state drawdown at 15 fully penetrating observation wells Self-potential geophysical response at 89 electrodes	Steady-state responses jointly analyzed with heterogeneous unconfined 3-D numerical model (MODFLOW)	Spatially distributed K	5.60E-05	3.00E-04	1.30E-03	*Straface et al.* [2011]
2008	Natural diurnal evapotranspiration and influx from river.	Transient head change responses at 1 fully penetrating well	Transient response separately analyzed with homogeneous, unconfined aquifer analytical model	Effective aquifer K (assumed isotropic)	N/A	3.40E-04	N/A	*Malama and Johnson* [2010]
2008–2009	518 partially penetrating (0.3 m) slug tests. Slug Range: 0.05–0.3 m (pneumatic).	Transient slug response at testing interval	Transient responses separately analyzed with homogeneous analytical model	Effective aquifer K (assumed isotropic)	3.30E-05	9.80E-04	5.60E-03	*Cardiff et al.* [2011][c]
2010	12 partially penetrating (1 m) pumping tests. Flow Rate Range: 20-30 L/min.	Transient head change responses at 21–28 partially penetrating (1 m) intervals per test	Transient responses jointly analyzed with numerical modeling of unconfined, heterogeneous K aquifer (MODFLOW)	Spatially distributed K	3.40E-05	3.00E-04	1.30E-03	This work

[a]Either heterogeneous, or "effective" for full aquifer.
[b]Approximate ranges given. Several models of heterogeneity tested, but all centered approximately around this K interval.
[c]Values given are for analysis case without wellbore skin.

on prior experimentation, the pumping periods and rates used are known to be sufficient to capture early time and start of late time behavior for the unconfined aquifer at the BHRS [*Barrash et al.*, 2007], but short enough to be efficient for running many tests while avoiding measureable effects of leakage from the river or superimposed drawdown from ET. Likewise, the pumping rate is sufficient to allow measureable signal propagation between adjacent wells without excessive drawdown in the pumping zone.

[18] The field system used in 2010 was selected and designed for collecting data simultaneously from a variety of types of instruments with logistical tractability (i.e., efficient installation time, minimal supporting equipment, and simplicity in operation and maintenance). Equipment for measurement, stimulation, and data acquisition consisted of modular components for flexibility in configuration and for portability to, from and within the site. Key components include: in-well packers and ports, fiberoptic pressure transducers with associated light conditioner electronics, strain gauge transducers, digital in-line flowmeter, straddle packer for pumping zone with transducers, and an external surface jet pump.

[19] The data acquisition system, or DAQ, used to collect all data consists of a modular rack-mounted system (National Instruments NI-CompactDAQ) for sampling and recording from all data sources, including the strain gauge transducers, fiberoptic transducers, and in-line flowmeter. The DAQ system is controlled by custom interactive software (developed by the authors), written in Labview. The DAQ control software allows input and storage of calibration parameters for all instruments in the field, contains flexible visualization routines for monitoring pretest and during-test responses, and stores all data collected to a single, time-referenced data file that can be easily treated and interpreted.

[20] Testing was carried out on the weekdays from 30 July through 6 August 2010. In terms of field effort, setup of all HT equipment required 2 days (30 July and 2 August) which included installation and pressurization of all multilevel packer-and-port assemblies in observation wells, with seven observation intervals per well, as well as a straddle-packer and extension risers installed in the first pumping well. Active testing began on 3 August starting from the bottom 1 m packed-off interval of well B4. Pumping proceeded at a constant rate per test, routinely $0.3 - 0.45\,\mathrm{L\,s^{-1}}$. The pumping interval was progressively raised by 1 m increments and pumping repeated at each new interval until the full saturated thickness had been tested, which was completed on 4 August. Following this, the straddle-packer pump assembly was removed from well B4 and installed in well B5, and then a similar full set of pumping tests for well B5 was carried out during 5 and 6 August. Figure 2 is a diagram illustrating the location of pumped intervals and observation intervals during this field campaign. An example of data collected during the field campaign can be seen in Figure 3, which shows the response of pressure sensors at all depths in well B1 to pumping from a 1 m interval near the bottom of well B4 (located laterally 5.6 m away). We note that responses are coherent even in the range where drawdown is on the order of a few millimeters.

3. Analysis Methodology

[21] In this work, we follow the approach developed by *Cardiff and Barrash* [2011] for inversion of transient HT

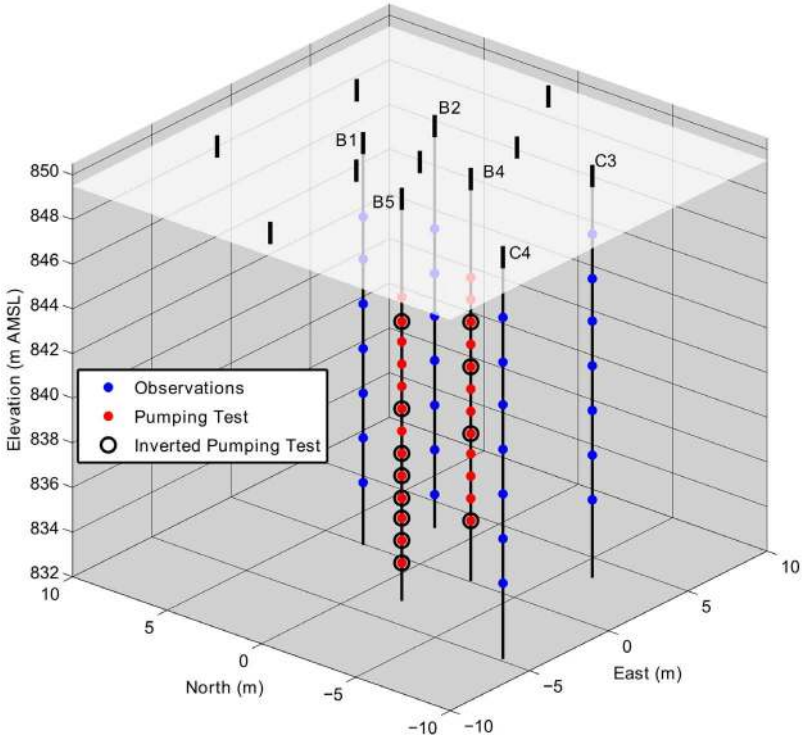

Figure 2. Testing configuration during August 2010 3DTHT field experiments. Locations of all A, B, and C wells shown at surface for reference, with A1 representing the origin (also shown in overhead view in Figure 1).

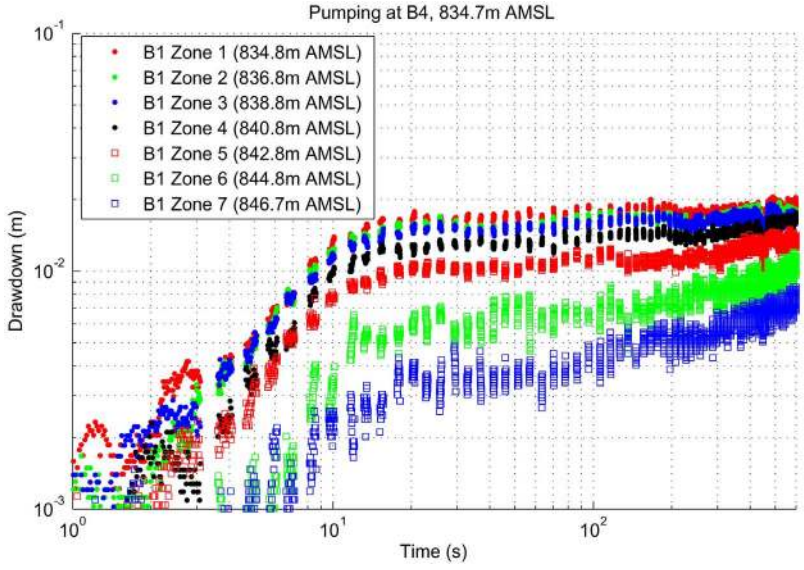

Figure 3. A sample data set, showing depth-dependent responses of transducers to a 3-D pumping stimulation (from time after pump start). Lateral spacing between pumping well B4 and observation well B1 is 5.5 m. Elevation difference between sensors and pumped interval ranges from 0–12 m, resulting in overall distances of 5.5–13.2 m.

data in unconfined aquifers. In this section, we briefly review both the numerical "forward" model used to simulate the tests performed and the inversion routine used to fit observation data (i.e., history matching).

3.1. Forward Model

[22] For our numerical models, we utilize the popular, fast and well-validated MODFLOW groundwater flow simulator [*Harbaugh*, 2005], which is capable of modeling saturated unconfined flow in water table aquifers (although it should be noted, the basic version of MODFLOW that we use does not take into account delayed vadose zone response, which is assumed negligible for our case). For modeling the BHRS 3DTHT tests of August 2010, a 60 m $\times$ 60 m areal extent is modeled, 18 m thick and centered on well A1, with boundaries oriented roughly parallel and perpendicular to the Boise River. Within the modeling domain, the maximum cell size is 1 m $\times$ 1 m $\times$ 0.6 m, with a high degree of refinement of the numerical grid in the roughly 10 m $\times$ 10 m central area where pumping and observations take place. The lateral boundaries of the modeling domain are set to constant head boundaries, the bottom of the domain is a no-flux boundary, and the top of the modeling domain is the water table (a free boundary), and is dealt with by MODFLOW as described in the user documentation [*Harbaugh*, 2005].

[23] The models contain roughly two million cells, and are run in a transient mode to produce simulated drawdown curves at monitoring wells. The models were designed using the GMS graphical user interface, then exported into standard MODFLOW input files. Once exported, the models were solved using a modified version of MODFLOW that includes the ADJ (adjoint) sensitivity process [*Clemo*, 2007], discussed further in section 3.2. Such forward models routinely required between $2 - 10$ min to run using a single core on a modern PC, and utilized less than 0.5 GB of RAM. Before inverse modeling, preliminary modeling was performed to evaluate the impact of boundary conditions. This modeling of short, relatively low flowrate tests similar to those performed at the BHRS indicated that boundary effects on observed drawdown curves are minimal when the boundaries are located at a distance of 30 m or more from the center of the testing area.

3.2. Inversion Method

[24] We utilize a modified version of the inversion routine described in the work of *Cardiff and Barrash* [2011] for fitting transient pumping-test data in unconfined aquifers (Figure 4). Our approach consists of a three-level inversion that produces estimates of geostatistical parameters as part of the inversion, in addition to estimating spatially distributed hydraulic conductivity (K) and assumed homogeneous values for specific storage and specific yield (S_s and S_y, respectively). While spatially distributed S_s and S_y can also be estimated with this approach, the synthetic results of *Cardiff and Barrash* [2011] showed that assuming constant storage parameters can reduce computational time and does not significantly affect K estimates (if reasonable ranges of storage parameter variability are assumed). The method is briefly reviewed here, with additional technical details found in the work of *Cardiff and Barrash* [2011].

[25] Algorithmically, the method begins with the user providing: (1) $\mathbf{y}$ $(n \times 1)$, a vector containing an initial set of field data to fit (a few representative data points from each drawdown curve); (2) θ_s and θ_y, vectors containing initial estimates of geostatistical parameters for the aquifer's heterogeneity (i.e., variance and correlation lengths of the variogram) and the data error variances, respectively; and (3) $\mathbf{s}_p$ $(m \times 1)$, an initial guess for the aquifer parameters (usually a homogeneous starting point).

[26] The innermost loop of the program solves the quasi-linear geostatistical inversion of *Kitanidis* [1995], with modifications for large-scale problems. For a problem with

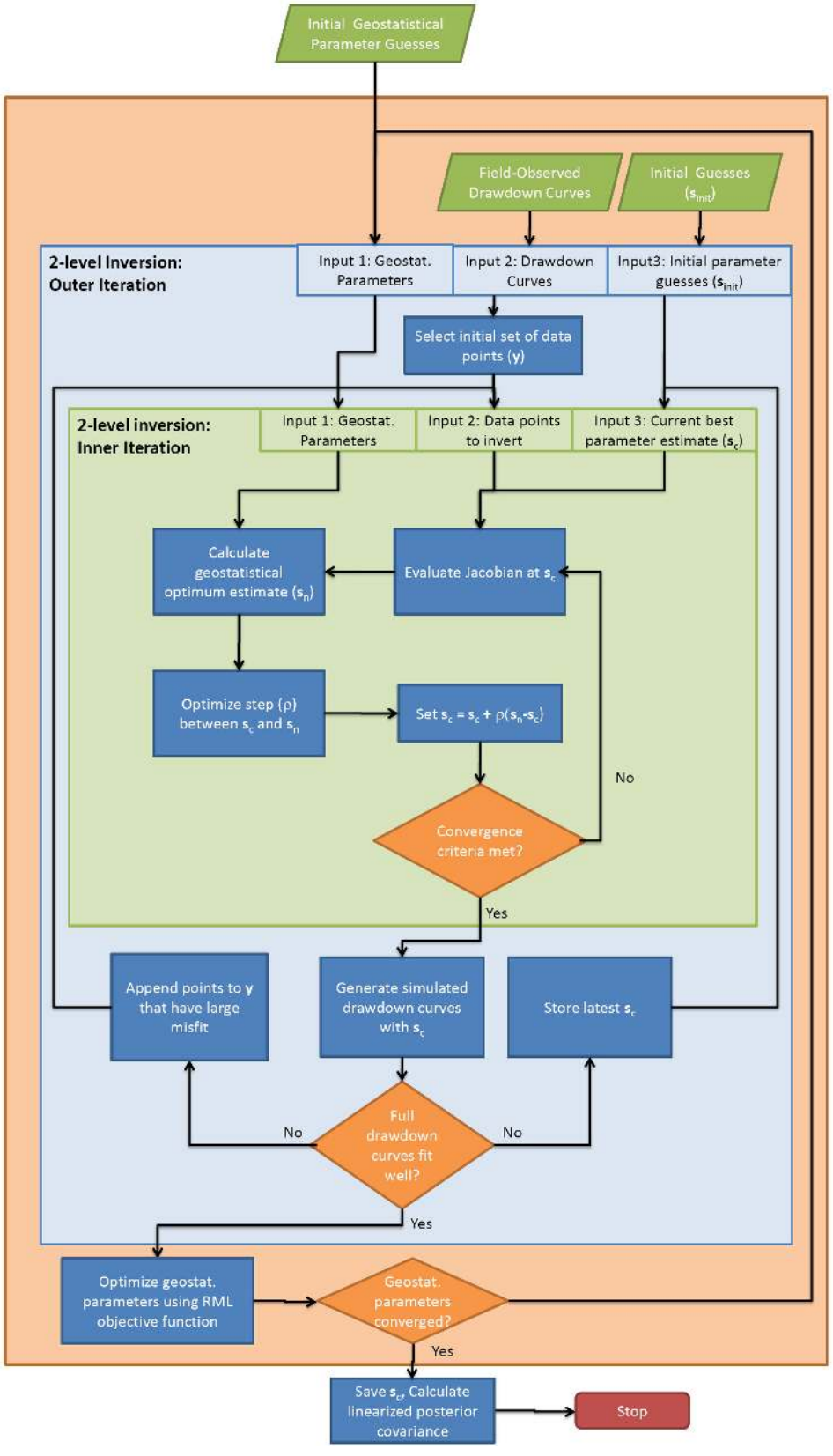

Figure 4. Flowchart illustrating 3-level strategy for inversion of field data including estimation of geostatistical "structural" parameters.

forward model **h** which takes as input parameter vector **s** $(m \times 1)$ and outputs a set of $(n \times 1)$ measurements, one calculates the $(n \times m)$ Jacobian $\tilde{\mathbf{H}}_{(i,j)} = \frac{\partial \mathbf{h_i}}{\partial \mathbf{s_j}}|_{\mathbf{s}_p}$ (where $\mathbf{s}_p$ is the current parameter vector guess) and then solves the linearized geostatistical parameter estimation equations to obtain a new estimate, denoted $\mathbf{s}_c$:

$$\mathbf{s}_c = \mathbf{X}\beta + \mathbf{Q}(\theta_\mathbf{s})\hat{\mathbf{H}}^T\xi,$$

where ξ $(n \times 1)$ and β $(p \times 1)$ are found through solution of the equation:

$$\begin{bmatrix} \tilde{\mathbf{H}}\mathbf{Q}(\theta_\mathbf{s})\hat{\mathbf{H}}^T + \mathbf{R}(\theta_y) & \tilde{\mathbf{H}}\mathbf{X} \\ (\tilde{\mathbf{H}}\mathbf{X})^T & \mathbf{0}_{p\times p} \end{bmatrix} \begin{bmatrix} \xi \\ \beta \end{bmatrix} = \begin{bmatrix} \mathbf{y} - \mathbf{h}(\mathbf{s}_p) + \tilde{\mathbf{H}}\mathbf{s}_p \\ \mathbf{0}_{p\times 1} \end{bmatrix}$$

and where $\mathbf{Q}(\theta_s)$ is the $(m \times m)$ parameter covariance matrix calculated using the current estimates of the geostatistical parameters (θ_s); $\mathbf{R}(\theta_y)$ is the $(n \times n)$ data error covariance matrix calculated using the current estimates of the data error variances (θ_y); and $\mathbf{X}$ is the $(m \times p)$ matrix of drift coefficients. A line search is performed between $\mathbf{s}_p$ and $\mathbf{s}_c$, and the process is repeated until convergence.

[27] At the second level of the code, a full drawdown curve is generated from the forward model using the best parameter estimates from the innermost loop. If parts of the drawdown curve are not well fit, additional data points are added to the data vector and the innermost loop of the code is rerun. This second-level iteration loop continues until all times of all drawdown curves are deemed acceptably fit.

[28] Finally, at the third and outermost level, the code optimizes the Restricted Maximum Likelihood (RML) objective function for estimating geostatistical structural parameters and data error variances, which was shown by *Kitanidis* [1995] to be an unbiased estimator of these parameters for linear inverse problems. Given the Jacobian matrix (denoted $\hat{\mathbf{H}}$) evaluated at the best parameter estimates (denoted $\hat{\mathbf{s}}$), the following RML objective function is numerically optimized to obtain improved estimates of θ_s and θ_y:

$$\min_{\theta_s,\theta_y} \frac{1}{2}\ln|\Psi| + \frac{1}{2}\ln|\mathbf{X}^T\hat{\mathbf{H}}^T\Psi^{-1}\hat{\mathbf{H}}\mathbf{X}| + \frac{1}{2}\left(\mathbf{y} - \mathbf{h}(\hat{\mathbf{s}}) + \hat{\mathbf{H}}\hat{\mathbf{s}}\right)^T \left(\Psi^{-1} - \Psi^{-1}\hat{\mathbf{H}}\mathbf{X}(\mathbf{X}^T\hat{\mathbf{H}}^T\Psi^{-1}\hat{\mathbf{H}}\mathbf{X})^{-1} \mathbf{X}^T\hat{\mathbf{H}}^T\Psi^{-1}\right)\left(\mathbf{y} - \mathbf{h}(\hat{\mathbf{s}}) + \hat{\mathbf{H}}\hat{\mathbf{s}}\right)^T$$

where $\Psi = \hat{\mathbf{H}}\mathbf{Q}(\theta_s)\hat{\mathbf{H}}^T + \mathbf{R}(\theta_y)$. If θ_s or θ_y change significantly, the values are returned to the inner two-level iteration section again, otherwise the program is exited and convergence is declared, at which point linearized posterior uncertainty estimates are generated.

[29] For most large-scale inverse modeling approaches, the most computationally time-consuming step is evaluation of parameter sensitivities, i.e., the model Jacobians. In our approach, sensitivities of observations to parameters are calculated using the ADJ sensitivity process for MODFLOW designed by *Clemo* [2007], which for a particular test requires one forward model run and n adjoint model runs, where n is the number of observations for the given test, and for which adjoint model runs are comparable in speed to standard forward model runs. In contrast, simple computation of sensitivities via, e.g., finite difference approximations require at least $m + 1$ forward model runs, where m is the number of parameters being estimated. In cases where the parameters being estimated represent spatially distributed values at a large number of locations, generally $m >> n$. Thus, the approach of using the ADJ process for imaging problems results in drastic computational savings when compared with traditional (e.g., finite difference) sensitivity evaluations. In addition, the inner two-level inversion strategy, as described in further detail in the work of *Cardiff and Barrash* [2011], increases computation efficiency by keeping the number of observations inverted (n) as low as possible, and only adding observations to the inversion as needed to improve fit of the full drawdown curve.

4. Application to Field Data

[30] In this section, we discuss the particulars of data processing and application of the above-described 3DTHT methodology to the field data collected during the August 2010 3DTHT field experiments. We then compare the results of the inversion to results obtained during previous characterization efforts.

4.1. Data Processing

[31] Visual evaluation of all drawdown curves obtained during field testing was used to select a subset of high-quality data for use in inverse modeling. Data from FO transducers which displayed significant drift (generally seen in previous-generation transducers) were filtered out, as were tests where significant variability in the pump flowrate occurred during testing. While tests with nonconstant flowrates can be inverted using our methodology, they would require a high degree of temporal discretization in MODFLOW and thus result in much slower-running models. For this reason, we have chosen not to invert the data from such tests, and have focused field efforts on reducing early time pump variability for future testing. The final high-quality subset of data selected for inversion consists of a total of 265 drawdown curves from the reliable subset of strain gauge transducers and FO transducers measured during 12 different pumping tests (approximately half of the tests run during the field campaign).

[32] From the selected data, a set of three data points was picked from each drawdown curve (using early time, intermediate-time and late-time data points from the drawdown curves) and these data points were used to initialize the inversion strategy discussed above. An anisotropic exponential covariance model, oriented with principal components parallel to the model grid directions, was assumed and initial covariance parameters were also input into the inversion strategy (Table 3). Additionally, we assumed a stationary mean for the parameter field investigated, meaning that the matrix **X** described above consisted of an $(m \times 1)$ vector of 1s. Using these inputs, the two-level inversion strategy was run until convergence of inner iterations (as discussed in the work of *Cardiff and Barrash* [2011]), and additional outer iterations were performed if full drawdown curve data fit was poor. We have assumed during inversion that the parameters S_y and S_s are roughly

Table 3. Initial Guess Used for Geostatistical "Structural" Parameters, Final Inversion Estimate, and Estimate Obtained During Previous Slug Testing[a]

	Initial Guess for Inversion	Final Inversion Estimate	Slug Testing Estimate
σ^2	0.1	0.23	0.14
L_x	5	18	10
L_y	5	8	6
L_z	5	1.2	1.5

[a]Geostatistical model assumed is exponential, with correlation lengths oriented perpendicular and parallel to the Boise River (x and y, respectively), and vertically (z).

constant and thus only invert for spatial variability in hydraulic conductivity, K. While variability in both S_y and S_s is expected in this real-world aquifer, the degree of variability is believed to be much less than the variability in K.

4.2. Results of Inversion

[33] Our inversion represents one of the larger-scale 3DTHT numerical computations performed that we are aware of, with 796 observations inverted and a parameter field that includes 111,630 spatially distributed K values to be estimated (in addition to assumed-homogeneous S_s and S_y values). Runtime required for completion of the inner two levels of the inversion varied according to the nonlinearity encountered and other factors, but could generally be carried out in 48–72 h using 6 processor cores on a single computer with 12GB of RAM. This time required represents the total compute time when a given set of geostatistical structural parameters are used, and is thus comparable to runtime reported in other studies where geostatistical parameters are often assumed known during inversion (e.g., recent studies by *Illman et al.* [2009], *Berg and Illman* [2011], *Huang et al.* [2011]). While still numerically intensive and requiring significant computing time, we note that the results obtained herein are significantly more efficient than those discussed in other recent studies. For example, the study of *Berg and Illman* [2011], which is similar in many regards, estimated spatially distributed K and S_s values at 32,768 spatial locations and required more than one week of computing time to invert 4 tests using between 8 and 40 processors on a PC cluster with 12 quad-core slave nodes and 16GB RAM per slave.

[34] Sensitivity calculation was, by far, the most computationally intensive step in the inversion process. The full sensitivity matrix, consisting of sensitivities of ≈800 observations to changes in ≈110,000 parameters required roughly 11 h of computational time. We found consistently that good fits to *all* data points were obtained by inverting only the selected subset of 3 data points per drawdown curve as discussed above—a similar result to the numerical experiments presented in the work of *Cardiff and Barrash* [2011]. Thus, the second level of the inversion consistently required only a single iteration. Runtime required by the outermost iteration level was generally between 1–3 h in order to estimate geostatistical structural parameters.

[35] The imaging results from our inversion are shown graphically (from two different perspectives) in Figures 5a and 6a. For this case, the geostatistical parameters estimated during inversion are shown in Table 3. At the completion of inversion, the root mean square error (RMSE) between inverted data points and simulated data points was 1.8 mm; a crossplot between all inverted data points and the comparable simulated data after inversion is shown in Figure 7. The RMSE for *all* collected data points (i.e., the full field drawdown curve datasets as shown in Figure 3)

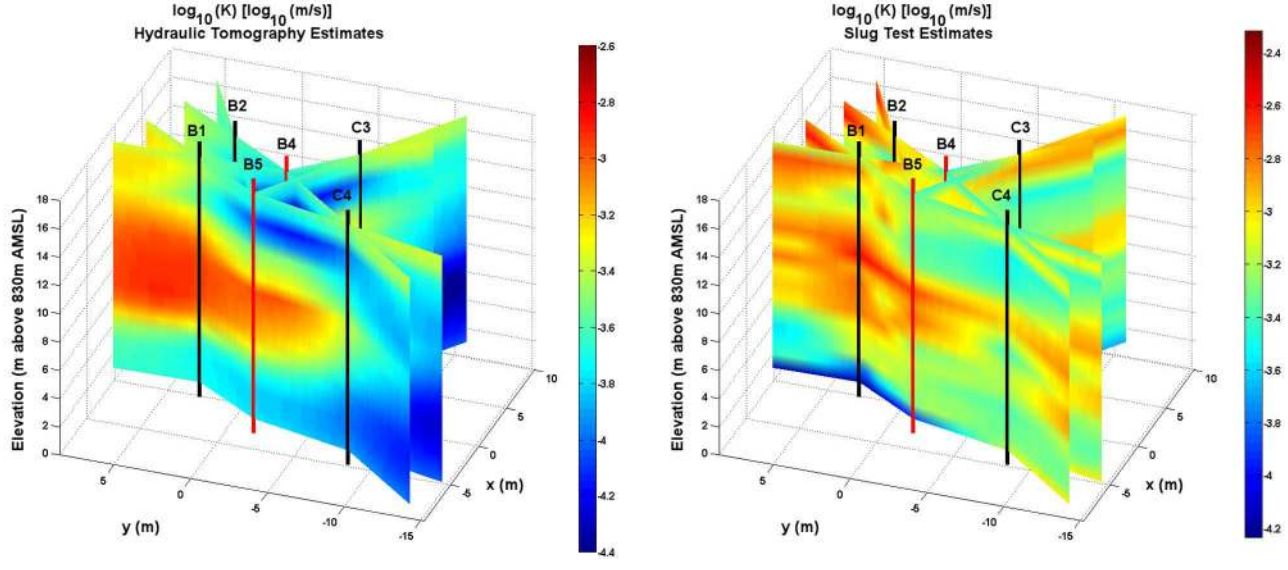

Figure 5. Comparison between $\log_{10}(K)$ estimates obtained from 3-D hydraulic tomography analysis and $\log_{10}(K)$ estimates from kriging of slug test results. View from the west shows values along slice-planes connecting pumping wells (red) and observation wells (black). Note scales, which range from minimum to maximum $\log_{10}(K)$ value for each set of estimates, are different; this is used to better highlight similarities in distributions of relative K estimate magnitudes, and to de-emphasize slight high bias in slug test results.

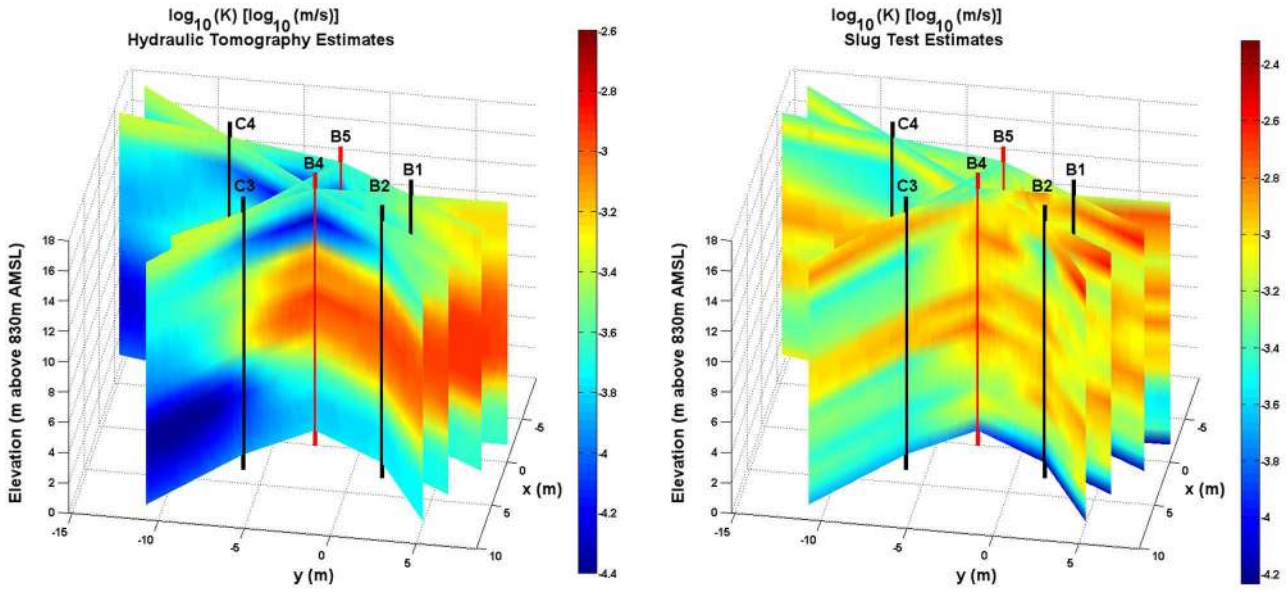

Figure 6. Comparison between $\log_{10}(K)$ estimates obtained from 3-D hydraulic tomography analysis and $\log_{10}(K)$ estimates from kriging of slug test results. View from the east shows values along slice-planes connecting pumping wells (red) and observation wells (black). Note scales, which range from minimum to maximum $\log_{10}(K)$ value for each set of estimates, are different; this is used to highlight similarities in relative estimate magnitudes.

was 2.2 mm; cross-plots of all collected data versus the comparable simulated data are shown on a test-by-test basis in Figure 8. As another way of visualizing the quality of data fit, a comparison of simulated versus observed drawdown curves at all observation intervals for one pumping test is shown in Figure 9. Given the variety of errors present in field datasets—which includes instrument noise of $\sigma \approx 1$ mm in addition to errors associated with exact instrument positioning, boundary condition assumptions, imperfect measurement/modeling of pumping flow rates, etc.—we believe this represents an excellent fit to the observations. In Figure 10, we present results of the first-order uncertainty analysis provided by the geostatistical inversion strategy for the $\log_{10}(K)$ estimates obtained using the 3DTHT data; this analysis can be used as a guide to assess imaging confidence or suggest further data collection areas.

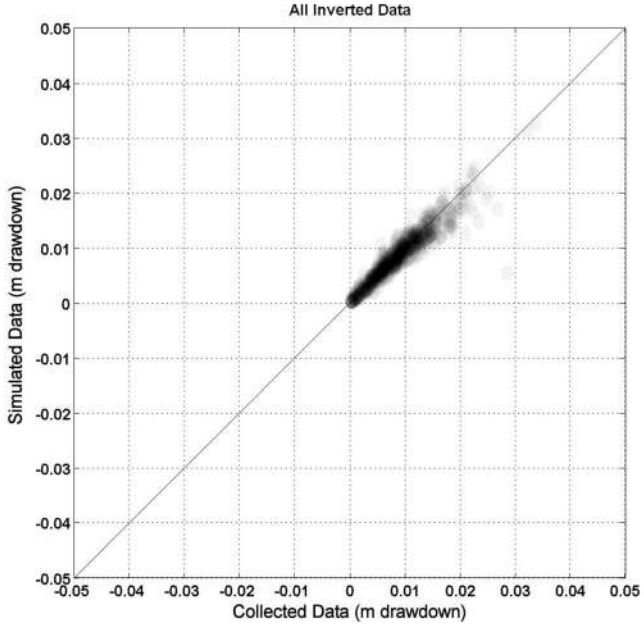

Figure 7. Crossplot of inverted data from all pumping tests, showing fit to each of the 3 points chosen per drawdown curve. Points are plotted as transparent to highlight relative density of points near perfect fit line.

[36] The results of K characterization efforts from 3DTHT are paired against comparable maps (Figures 5b and 6b) of estimated K based on kriged results from earlier slug testing conducted at 0.3 m intervals in all wells [*Cardiff et al.*, 2011]. Likewise, we also present a comparison of the K estimate profiles obtained at wellbores from slug testing against 3DTHT estimates at those locations in Figure 11, which show similar overall trends. The geostatistical parameters derived from analysis of the slug tests can also be compared with those estimated during inversion (Table 3), and show good agreement. The overall patterns of heterogeneity observed are very similar (especially in terms of large-scale features) in both datasets, though the overall values of K obtained by slug tests are generally higher, by a factor of ≈ 3. Based on prior studies at the BHRS that have obtained similar K magnitudes to those found by 3DTHT (including the tracer test analysis of *Daffon et al.* [2011b] and the 2-D HT analysis of *Cardiff et al.* [2009]), we believe that the K estimates obtained via slug testing are slightly biased toward overly high-K estimates. Such a bias can be introduced by several assumptions or inaccuracies in the model used during slug test analysis, e.g., the "effective length" associated with the slug testing flow geometry (e.g., see discussion in the work of *Cardiff*

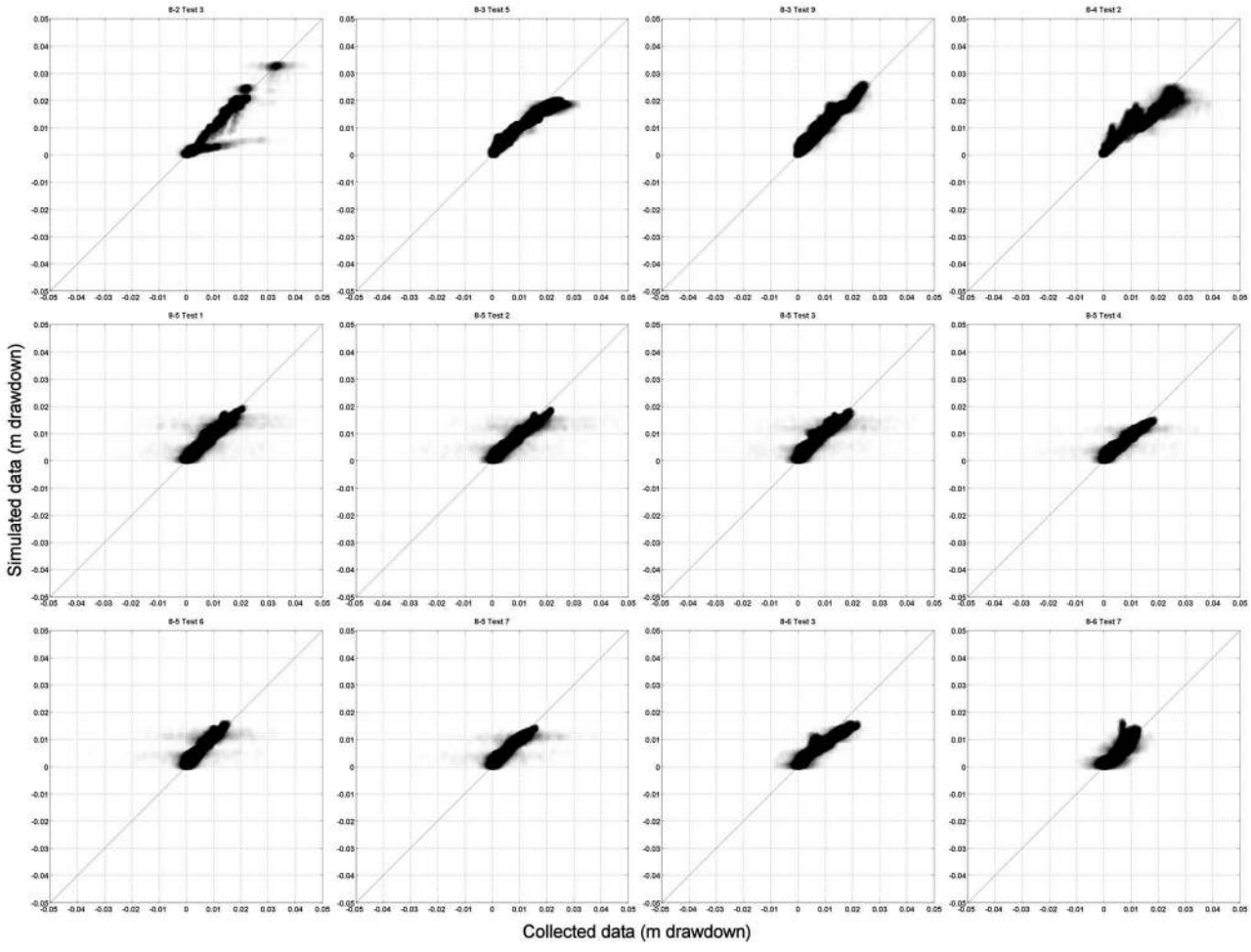

Figure 8. Cross-plots of all collected datapoints for 12 tests analyzed versus all simulated data from forward model (one pumping test per plot). Points are plotted as transparent to highlight relative density of points clustered near the perfect fit line.

et al. [2011], for examples of how slug test analyses can be biased by modeling assumptions). The fine-scale details of heterogeneity obtained with slug testing could not be completely validated against the 3DTHT data, due to the sparseness of 3DTHT observation locations in boreholes from the limited proof-of-concept testing of this study. However, the overall trends of K values observed from slug testing are consistent with those observed via 3DTHT.

[37] As one cross-validation method, we imported the kriged K field obtained from slug test estimates into our numerical models and performed an inversion of the field data in which the only parameters estimated were linear rescaling coefficients used to modify the obtained slug-test values. That is, we assumed K heterogeneity throughout the parameter field was equal to

$$\log_{10}\left(K(\mathbf{x})\right) = \frac{\log_{10}\left(K_{slug}(\mathbf{x})\right)}{\left[\max\left(\log_{10}\left(K_{slug}(\mathbf{x})\right)\right) - \min\left(\log_{10}\left(K_{slug}(\mathbf{x})\right)\right)\right]}\alpha + \beta,$$

where $K(\mathbf{x})$ is the hydraulic conductivity used in the numerical model at a point in space, $K_{slug}(\mathbf{x})$ is the kriged slug estimate of K obtained at that point in space; $\min()$ and $\max()$ represent the minimum and maximum values obtained throughout the spatial domain; and α and β are the parameters estimated by inversion in this case. Using this technique, the rescaled K estimates obtained from slug testing were able to fit the 3DTHT data with an RMSE of 3.5 mm; in comparison, the best fit obtained between field data and a homogeneous numerical model had an RMSE of 6 mm. Both of these lines of evidence suggest that the 3DTHT tests of 2010 are sensing the same overall pattern of heterogeneity sensed during earlier slug testing at the BHRS, and that the heterogeneity detected by the 3DTHT tests is "significant," in the sense that the 3DTHT tests cannot be adequately fit using a homogeneous aquifer model. However, the need for rescaling of the slug test values in order to fit 3DTHT data suggests that choices made during slug test data processing can highly impact the accuracy of these estimates (though we believe the relative rank order of estimates obtained is accurate).

5. Summary, Conclusions, and Future Work

[38] In this work, we present results of inversion of a series of tests from a proof-of-concept 3DTHT field campaign using modular, temporarily installed hydraulic

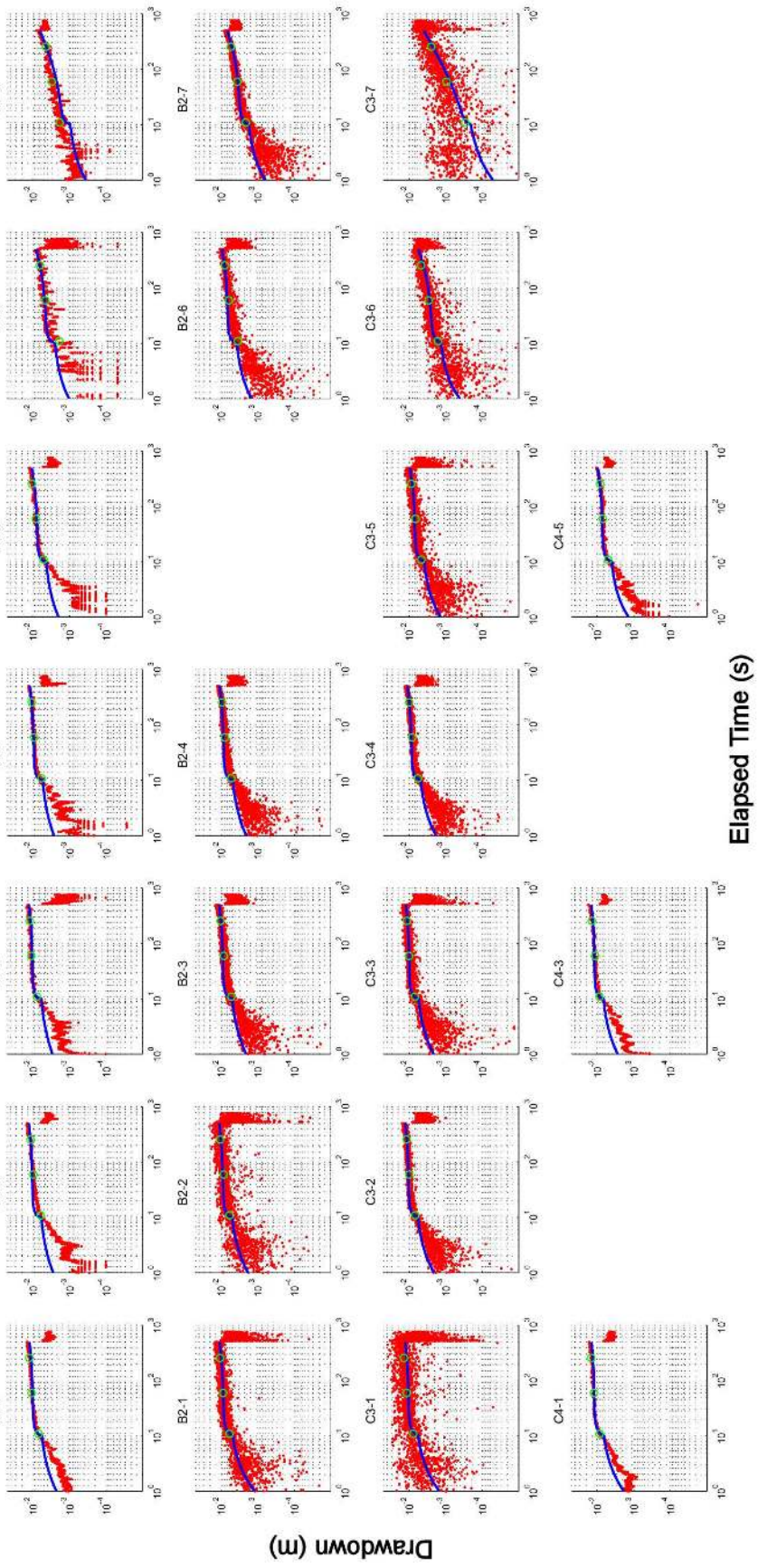

Figure 9. Comparison between observed datapoints (red dots) and simulated drawdown curves (blue lines) for a sample test, using K estimates obtained from inversion. Datapoints inverted are shown in green.

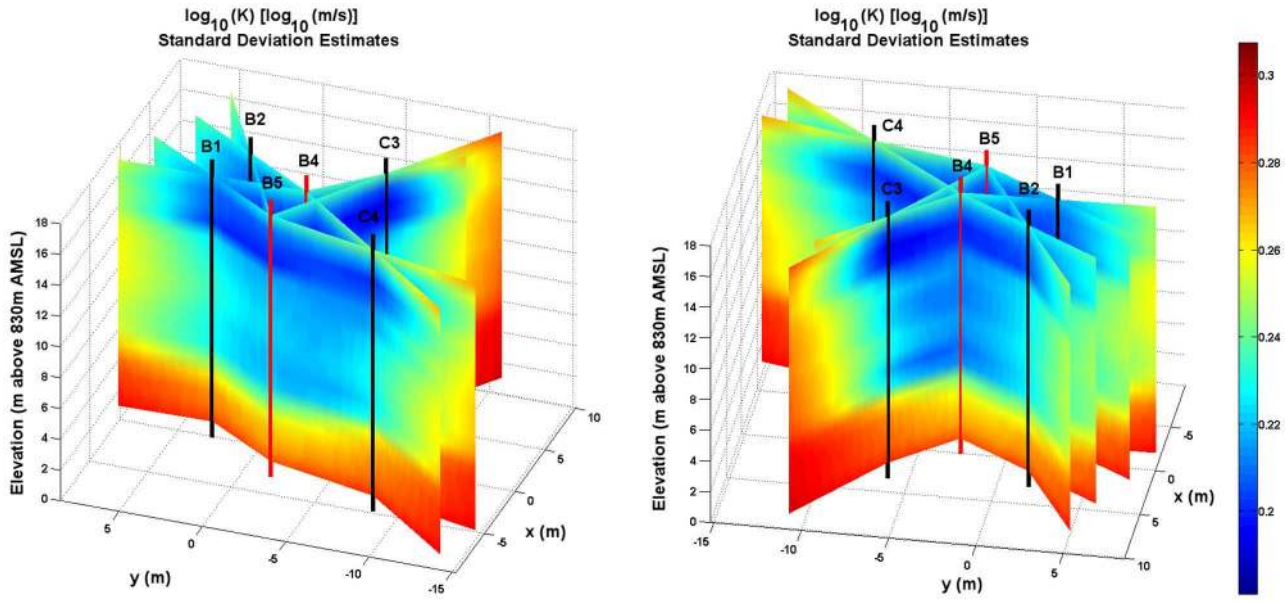

Figure 10. Estimated uncertainty in HT $\log_{10}(K)$ estimates, represented as standard deviation. Calculated using square root of diagonal of posterior covariance matrix using geostatistical theory.

tomography equipment to perform short-duration partially penetrating pumping tests at the BHRS. To analyze our collected data, a three-level inversion strategy was utilized which estimates spatially distributed hydraulic conductivity values in addition to the variances and correlation lengths associated with the parameter field. The estimates of heterogeneity obtained via 3DTHT were compared with estimates obtained during a previous high-resolution distributed K

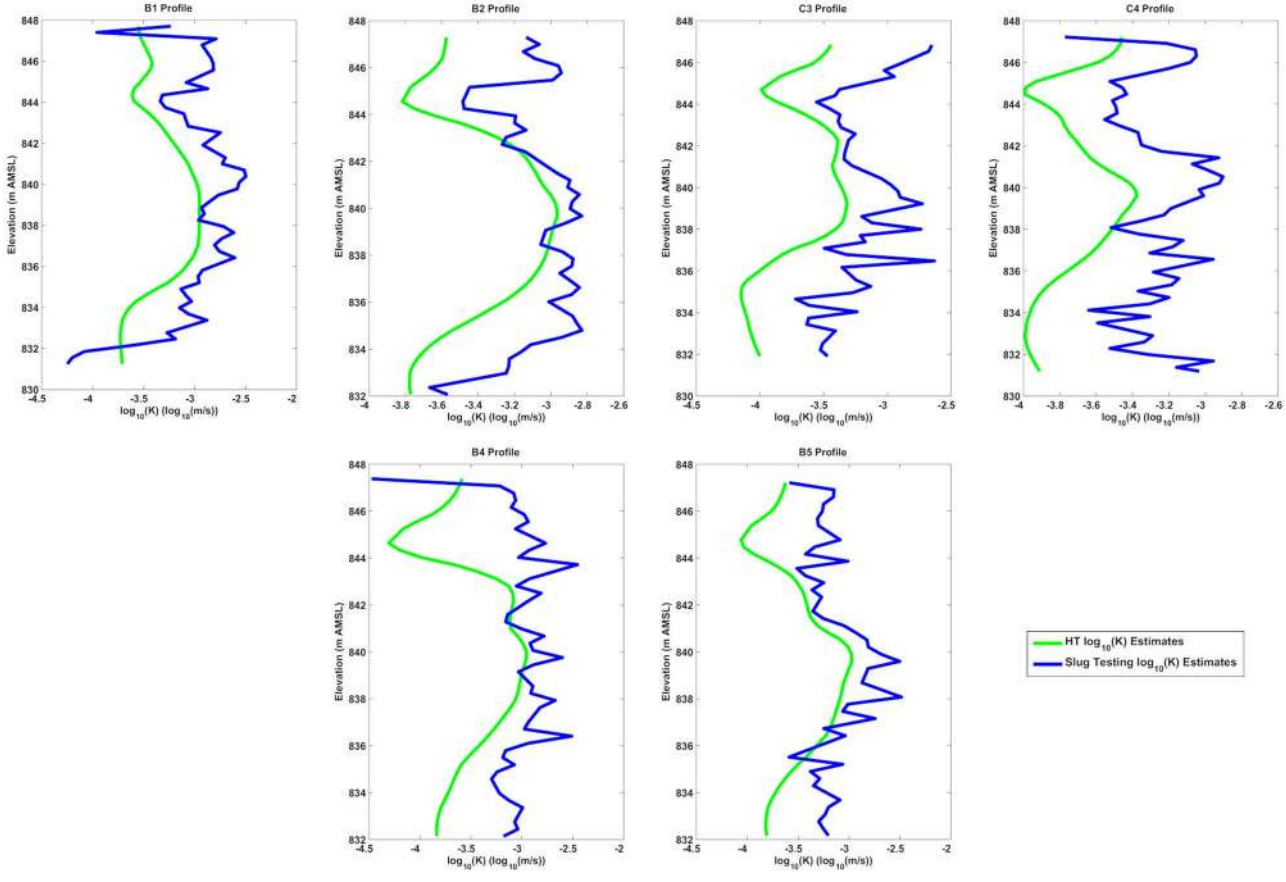

Figure 11. Comparison between slug test K estimate profiles obtained at wellbores and 3DTHT K estimates. Top row represents observation wells, and bottom row represents pumping wells.

estimation study which utilized partially penetrating slug tests to characterize the BHRS aquifer. Overall, we find that the general pattern of heterogeneity is consistent between these two strategies. However, the slug test estimates appear to be biased toward overly high hydraulic conductivity, but can be made to fit the 3DTHT data relatively well by a linear rescaling of the $\log_{10}(K)$ estimates, suggesting that the overall patterns of relative K magnitude obtained with slug testing are reasonable.

[39] As discussed in the work of *Cardiff and Barrash* [2011], the K values obtained through slug testing do not correlate overall with porosity values measured or estimated at the BHRS via neutron porosity logging, GPR and other methods. Since the 3DTHT imaging results appear to be, overall, consistent with patterns of heterogeneity seen in slug testing, the 3DTHT data provide an additional line of evidence that the relative K trends obtained in that work are reasonable and that K and porosity are not well-correlated uniformly throughout the BHRS.

[40] While still only at the proof-of-concept stage, we believe that the 3DTHT survey presented in this work, which included fitting of 265 drawdown curves from 12 pumping tests, and inverted for over 100,000 parameters, is one of the largest-scale 3-D HT studies presented to date. In a previous summary of HT work to date, *Cardiff and Barrash* [2011] found only three existing studies where 3-D HT field data were utilized to image 3-D aquifer parameters. These include (1) *Illman et al.* [2009], who inverted 35 drawdown curves from two pumping tests at the fractured-rock Mizunami Underground Research Site, Japan using a numerical model with 5184 nodes and inversion based on the successive sequential linear estimator (SSLE) code of *Zhu and Yeh* [2005]; (2) *Brauchler et al.* [2011], who analyzed 392 pulse travel-time-based tests in two different planes, using an asymptotic approximate forward model with 600 voxels that calculated raypath travel times and an inversion based on the SIRT algorithm [*Gilbert*, 1972]; and (3) *Berg and Illman* [2011], who analyzed $\approx$ 160 drawdown curves from four pumping tests using the HydroGeoSphere model [*Therrien et al.*, 2005] with 32,768 nodes, and again using the SSLE for tomographic inversion.

[41] A high-K unconfined system ($K_{avg} \approx 10^{-3}$–$10^{-4}\,\mathrm{m\,s^{-1}}$), the BHRS presents a relatively challenging environment for the application of 3DTHT because of the high hydraulic conductivity and only moderate K heterogeneity. This is because the deviations in pressure response resulting from heterogeneity (which provide the information content for hydraulic tomography) are relatively small—on the order of several mm—for high K, moderately heterogeneous systems, and for tests similar in dimension and stimulation magnitude to the tests presented here. Still, in this work, we were able to extract meaningful results from 3DTHT data by using a combination of high-sensitivity transducers and careful data analysis. In the future, improvements to instrument sensitivity as well as to pumping strategies that allow greater stimulation magnitude will help to produce even more accurate and higher-resolution estimates of heterogeneity. Efforts to perform higher-resolution and larger-scale characterization at the BHRS using 3DTHT are ongoing and numerous improvements to the full suite of equipment necessary to perform 3DTHT are being developed. As a guiding principle, the equipment being developed and improved is designed to be modular, temporary, portable, and durable for field implementation such that it can be installed to produce 3-D information at sites with standard fully penetrating wells or relatively long-screened wells. Based on experience with existing packer technology (used for isolating well depth intervals), we are developing an improved design that can be installed more quickly, allows larger numbers of monitoring intervals (with flexible length), and can be easily configured to allow multiple observation types per interval (e.g., pressure and solute concentration). For sensor technology, discussions with our instrument supplier for fiberoptic pressure transducers are resulting in designs with greater durability and accuracy. Similarly, our custom design data acquisition software and hardware is being upgraded to allow more simultaneous channels of data acquisition and to provide basic processing capabilities. Finally, while our current inversion was performed using only a single multicore PC, upscaling of the existing code to parallel computing platforms should allow inversions with significantly larger numbers of parameters, inclusion of larger characterization datasets, and analyses that are able to complete in a matter of hours. Though our first results from 3DTHT are quite promising and suggest consistency with other K characterization efforts, this represents only a first step toward detailed 3DTHT characterization that will doubtlessly improve with additional testing and optimization of the methodology.

[42] Another area for continuing research is study of the relative merits and drawbacks of various inversion strategies for hydraulic tomography. Other analysis approaches that could be applied to 3-D imaging of HT data include the steady-shape approach [*Bohling et al.*, 2002, 2007] and approaches based on temporal moments of drawdown [*Li et al.*, 2007]. With appropriate stimulation strategies, approximate but fast pulse travel-time-based approaches may be employed [e.g., *Brauchler et al.*, 2011], or other clever decompositions of signals may provide for faster analysis approaches. Indeed, as 3-D hydraulic tomography becomes more practical for field implementation through instrumentation, data collection, and computational advances, an interesting area of continuing research will be comparing the computational speed, effectiveness and robustness of the suggested approaches used to analyze collected HT data.

[43] **Acknowledgments.** Work at Boise State University was supported by NSF Awards 0710949 and 0934680, and by the US Army RDECOM ARL Army Research Office Award W911NF-09-l-0534. Work at Stanford was supported by NSF Award 0934596, Subsurface Imaging and Uncertainty Quantification. M. Cardiff and W. Barrash gratefully acknowledge students Michael Thoma and Brady Johnson for their assistance with the field experimentation discussed in this work. The authors also gratefully acknowledge comments from three anonymous reviewers, which helped improve this manuscript.

References

Alexander, M., S. J. Berg, and W. Illman (2010), Field study of hydrogeologic characterization methods in a heterogeneous aquifer, *Ground Water*, *49*, 365–382, doi:10.1111/j.1745-6584.2010.00729.x.

Asprion, U., and T. Aigner (1999), Towards realistic aquifer models: Three-dimensional georadar surveys of quaternary gravel deltas (singen basin, sw Germany), *Sediment. Geol.*, *129*, 281–297.

Barrash, W., and T. Clemo (2002), Heirarchical geostatistics and multifacies systems: Boise Hydrogeophysical Research Site, Boise, Idaho, *Water Resour. Res.*, *38*(10), 1196, doi:10.1029/2002WR001436.

Barrash, W., and E. C. Reboulet (2004), Significance of porosity for stratigraphy and textural composition in subsurface, coarse fluvial deposits:

Boise Hydrogeophysical Research Site, *Geol. Soc. Am. Bull.*, *116*, 1059–1073.

Barrash, W., T. Clemo, and M. D. Knoll (1999), Boise Hydrogeophysical Research Site (BHRS): Objectives, design, initial geostatistical results, in *Symposium on the Application of Geophysics to Engineering and Environmental Problems*, pp. 389–398, Environ. and Eng. Geophys. Soc., Oakland, Calif.

Barrash, W., T. Clemo, J. J. Fox, and T. C. Johnson (2006), Field, laboratory, and modeling investigation of the skin effect at wells with slotted casing, Boise Hydrogeophysical Research Site, *J. Hydrol.*, *326*, 181–198.

Barrash, W., T. Clemo, T. C. Johnson, C. Leven, B. Malama, and G. Nelson (2007), Hydraulic tomography at the Boise Hydrogeophysical Research Site, paper presented at SIAM Conference on Mathematical and Computational Issues in the Geosciences, Soc. for Ind. and Appl. Math., Santa Fe, N. M.

Bayer, P., P. Huggenberger, P. Renard, and A. Comunian (2011), Three-dimensional high resolution fluvio-glacial aquifer analog: Part 1: Field study, *J. Hydrol.*, *405*, 1–9.

Beckie, R., and C. F. Harvey (2002), What does a slug test measure: An investigation of instrument response and the effects of heterogeneity, *Water Resour. Res.*, *38*(12), 1290, doi:10.1029/2001WR001072.

Beres, M., A. Green, P. Huggenberger, and H. Horstmeyer (1995), Mapping the architecture of glaciofluvial sediments with three-dimensional georadar, *Geology*, *23*, 1087.

Berg, S., and W. Illman (2011), Three-dimensional transient hydraulic tomography in a highly heterogeneous glaciofluvial aquifer-aquitard system, *Water Resour. Res.*, *47*, W10507, doi:10.1029/2011WR010616.

Bohling, G. C. (1999), Evaluation of an induced gradient tracer test in an alluvial aquifer, Ph.D. dissertation, Univ. of Kansas, Lawrence.

Bohling, G. C. (2009), Sensitivity and resolution of tomographic pumping in an alluvial aquifer, *Water Resour. Res.*, *45*, W02420, doi:10.1029/2008WR007249.

Bohling, G. C., X. Zhan, J. J. Butler Jr., and L. Zheng (2002), Steady shape analysis of tomographic pumping tests for characterization of aquifer heterogeneities, *Water Resour. Res.*, *38*(12), 1324, doi:10.1029/2001WR001176.

Bohling, G. C., J. J. Butler Jr., X. Zhan, and M. D. Knoll (2007), A field assessment of the value of steady shape hydraulic tomography for characterization of aquifer heterogeneities, *Water Resour. Res.*, *43*, W05430, doi:10.1029/2006WR004932.

Bouwer, H., and R. Rice (1976), A slug test for determining hydraulic conductivity of unconfined aquifers with completely or partially penetrating wells, *Water Resour. Res.*, *12*, 423–428.

Bradford, J. H., W. Clement, and W. Barrash (2009), Estimating porosity with ground-penetrating radar reflection tomography: A controlled 3-D experiment at the Boise Hydrogeophysical Research Site, *Water Resour. Res.*, *45*, W00D26, doi:10.1029/2008WR006960.

Brauchler, R., R. Hu, T. Vogt, D. Al-Halbouni, T. Heinrichs, T. Ptak, and M. Sauter (2010), Cross-well slug interference tests: An effective characterization method for resolving aquifer heterogeneity, *J. Hydrol.*, *384*, 33–45.

Brauchler, R., R. Hu, P. Dietrich, and M. Sauter (2011), A field assessment of high-resolution aquifer characterization based on hydraulic travel time and hydraulic attenuation tomography, *Water Resour. Res.*, *47*, W03503, doi:10.1029/2010WR009635.

Butler, J. J., Jr. (1998), *The Design, Performance, and Analysis of Slug Tests*, Lewis Publ., Boca Raton, Fla.

Butler, J. J., Jr. (2002), A simple correction for slug tests in small-diameter wells, *Ground Water*, *40*, 303–307.

Butler, J. J., Jr., J. M. Healey, G. W. Mccall, E. J. Garnett, and S. P. I. Loheide (2002), Hydraulic tests with direct push equipment, *Ground Water*, *40*, 25–36.

Butler, J. J., Jr., P. Dietrich, V. Wittig, and T. Christy (2007), Characterizing hydraulic conductivity with the direct-push permeameter, *Ground Water*, *45*, 409–419.

Cardiff, M., and W. Barrash (2011), 3-D transient hydraulic tomography in unconfined aquifers with fast drainage response, *Water Resour. Res.*, *47*, W12518, doi:10.1029/2010WR010367.

Cardiff, M., W. Barrash, P. Kitanidis, B. Malama, A. Revil, S. Straface, and E. Rizzo (2009), A potential-based inversion of unconfined steady-state hydraulic tomography, *Ground Water*, *47*, 259–270.

Cardiff, M., W. Barrash, B. Malama, and M. Thoma (2011), Information content of slug tests for estimating hydraulic properties in realistic, high-conductivity aquifer scenarios, *J. Hydrol.*, *403*, 66–82.

Cho, J. S., J. T. Wilson, and F. P. J. Beck (2000), Measuring vertical profiles of hydraulic conductivity with in situ direct-push methods, *J. Environ. Eng.*, *126*, 775–777.

Clement, W., and W. Barrash (2006), Crosshole radar tomography in a fluvial aquifer near Boise, Idaho, *J. Environ. Eng. Geophys.*, *11*, 171–184.

Clement, W. P., and M. D. Knoll (2006), Traveltime inversion of vertical radar profiles, *Geophysics*, *71*, K67–K76.

Clement, W. P., W. Barrash, and M. D. Knoll (2006), Reflectivity modeling of a ground-penetrating radar profile of a saturated fluvial formation, *Geophysics*, *71*, K59–K66.

Clemo, T. (2007), Modflow-2005 ground water model - user guide to the adjoint state based sensitivity process (adj), technical report, Boise State Univ., Boise, Id.

Clifford, J., and A. Binley (2010), Geophysical characterisation of riverbed hydrostratigraphy using electrical resistance tomography, *Near Surf. Geophys.*, *8*, 493–501.

Conrad, S. H., R. J. Glass, and W. J. Peplinski (2002), Bench-scale visualization of dnapl remediation processes in analog heterogeneous aquifers: Surfactant floods and in situ oxidation using permanganate, *J. Contam. Hydrol.*, *58*, 13–49.

Cook, P., A. Love, N. Robinson, and C. Simmons (2005), Groundwater ages in fractured rock aquifers, *J. Hydrol.*, *308*, 284–301.

Crook, N., A. Binley, R. Knight, D. Robinson, J. Zarnetske, and R. Haggerty (2008), Electrical resistivity imaging of the architecture of substream sediments, *Water Resour. Res.*, *44*, W00D13, doi:10.1029/2008WR006968.

Curtis, G., P. Roberts, and M. Reihard (1986), A natural gradient experiment on solute transport in a sand aquifer: 4. Sorption of organic solutes and its influence on mobility, *Water Resour. Res.*, *22*, 2059–2067.

Dafflon, B., J. Irving, and W. Barrash (2011a), Inversion of multiple intersecting high-resolution crosshole GPR profiles for hydrological characterization at the Boise Hydrogeophysical Research Site, *J. Appl. Geophys.*, *73*, 305–314.

Dafflon, B., W. Barrash, M. Cardiff, and T. Johnson (2011b), Hydrological parameter estimations from a conservative tracer test with variable-density effects at the Boise Hydrogeophysical Research Site, *Water Resour. Res.*, *47*, W12513, doi:10.1029/2011WR010789.

Daley, T., E. Majer, and J. Peterson (2004), Crosswell seismic imaging in a contaminated basalt aquifer, *Geophysics*, *69*, 16.

Day-Lewis, F., J. Lane, and S. Gorelick (2006), Combined interpretation of radar, hydraulic, and tracer data from a fractured-rock aquifer near Mirror Lake, New Hampshire, USA, *Hydrogeol. J.*, *14*, 1–14.

Dekker, T., and L. M. Abriola (2000), The influence of field-scale heterogeneity on the infiltration and entrapment of dense nonaqueous phase liquids in saturated formations, *J. Contam. Hydrol.*, *42*, 219–251.

Dietrich, P., and C. Leven (2009), *Direct Push Technologies*, pp. 347–366, Springer, Berlin.

Dietrich, P., J. J. Butler Jr., and K. Faiss (2008), A rapid method for hydraulic profiling in unconsolidated formations, *Ground Water*, *46*, 323–328.

Doetsch, J., N. Linde, and A. Binley (2010a), Structural joint inversion of time-lapse crosshole ert and gpr traveltime data, *Geophys. Res. Lett.*, *37*, L24404, doi:10.1029/2010GL045482.

Doetsch, J., N. Linde, C. Ilaria, G. Stewart, and A. Green (2010b), Zonation for 3D aquifer characterization based on joint inversions of multi-method crosshole geophysical data, *Geophysics*, *75*, G53.

Einarson, M. D., and J. A. Cherry (2002), A new multilevel ground water monitoring system using multichannel tubing, *Ground Water Monit. Remed.*, *22*, 52–65.

Ellefsen, K., P. Hsieh, and A. Shapiro (2002), Crosswell seismic investigation of hydraulically conductive, fractured bedrock near Mirror Lake, New Hampshire, *J. Appl. Geophys.*, *50*, 299–317.

Ernst, J., A. Green, H. Maurer, and K. Holliger (2007), Application of a new 2D time-domain full-waveform inversion scheme to crosshole radar data, *Geophysics*, *72*, J53.

Fienen, M. N., P. K. Kitanidis, D. Watson, and P. Jardine (2004), An application of Bayesian inverse methods to vertical deconvolution of hydraulic conductivity in a heterogeneous aquifer at Oak Ridge National Laboratory, *Math. Geol.*, *36*, 101–126.

Freyberg, D. (1986), A natural gradient experiment on solute transport in a sand aquifer: 2. Spatial moments and the advection and dispersion of nonreactive tracers, *Water Resour. Res.*, *22*, 2031–2046.

Garabedian, S., D. LeBlanc, L. Gelhar, and M. Celia (1991), Large-scale natural gradient tracer test in sand and gravel, Cape Cod, Massachusetts: 2. Analysis of spatial moments for a nonreactive tracer, *Water Resour. Res.*, *27*, 911–924.

Genereux, D., and J. Guardiario Jr. (2001), A borehole flowmeter investigation of small-scale hydraulic conductivity variation in the Biscayne aquifer, Florida, *Water Resour. Res.*, *37*, 1511–1517.

Gilbert, P. (1972), Iterative methods for the three-dimensional reconstruction of an object from projections, *J. Theor. Biol.*, *36*, 105–117.

Harbaugh, A. (2005), Modflow-2005, the U.S. Geological Survey modular ground-water model – the ground-water flow process, technical report, U.S. Geol. Soc., Reston, Va.

Harvey, R., L. George, R. Smith, and D. LeBlanc (1989), Transport of microspheres and indigenous bacteria through a sandy aquifer: Results of natural-and forced-gradient tracer experiments, *Environ. Sci. Technol.*, *23*, 51–56.

Hess, A. E. (1986), Identifying hydraulically conductive fractures with a slow-velocity borehole flowmeter, *Can. Geotech. J.*, *23*, 69–78.

Hess, K. (1989), Use of a borehole flowmeter to determine spatial heterogeneity of hydraulic conductivity and macrodispersion in a sand and gravel aquifer, Cape Cod, Massachusetts, in *Proc. Conf. on New Field Techniques for Quantizing the Physical and Chemical Properties of Heterogeneous Aquifers*, edited by F. J. Molz et al., pp. 497–508, Natl. Water Well Assoc., Dublin, Ohio.

Hess, K., S. Wolf, and M. Celia (1992), Large-scale natural gradient tracer test in sand and gravel, Cape Cod, Massachusetts: 3. Hydraulic conductivity variability and calculated macrodispersivities, *Water Resour. Res.*, *28*, 2011–2027.

Huang, S.-Y., J.-C. Wen, T.-C. J. Yeh, W. Lu, H.-L. Juan, C.-M. Tseng, J.-H. Lee, and K.-C. Chang (2011), Robustness of joint interpretation of sequential pumping tests: Numerical and field experiments, *Water Resour. Res.*, *47*, W10530, doi:10.1029/2011WR010698.

Hubbard, S., K. Williams, M. Conrad, B. Faybishenko, J. Peterson, J. Chen, P. Long, and T. Hazen (2008), Geophysical monitoring of hydrological and biogeochemical transformations associated with Cr (vi) bioremediation, *Environ. Sci. Technol.*, *42*, 3757–3765.

Hyndman, D. W., and S. M. Gorelick (1996), Estimating lithologic and transport properties in three dimensions using seismic and tracer data: The Kesterson aquifer, *Water Resour. Res.*, *32*, 2659–2670.

Illman, W., X. Liu, S. Takeuchi, T.-C. J. Yeh, K. Ando, and H. Saegusa (2009), Hydraulic tomography in fractured granite: Mizunami underground research site, Japan, *Water Resour. Res.*, *45*, W01406, doi:10.1029/2007WR006715.

Irving, G. D., M. D. Knoll, and R. J. Knight (2007), Improving crosshole radar velocity tomograms: A new approach to incorporating high-angle traveltime data, *Geophysics*, *72*, J31–J41.

Jawitz, J., M. D. Annable, G. Demmy, and P. S. C. Rao (2003), Estimating nonaqueous phase liquid spatial variability using partitioning tracer higher temporal moments, *Water Resour. Res.*, *39*(7), 1192, doi:10.1029/2002WR001309.

Kabala, Z. J. (1993), The dipole flow test: A new single-borehole test for aquifer characterization, *Water Resour. Res.*, *29*, 99–107.

Kemna, A., J. Vanderborght, B. Kulessa, and H. Vereecken (2002), Imaging and characterisation of subsurface solute transport using electrical resistivity tomography (ERT) and equivalent transport models, *J. Hydrol.*, *267*, 125–146.

Kitanidis, P. K. (1995), Quasi-linear geostatistical theory for inversing, *Water Resour. Res.*, *31*, 2411–2419.

LeBlanc, D., S. Garabedian, K. Hess, and L. Gelhar (1991), Large-scale natural gradient tracer test in sand and gravel, *Water Resour. Res.*, *27*, 895–910.

Li, W., A. Englert, O. A. Cirpka, J. Vanderborght, and H. Vereecken (2007), Two-dimensional characterization of hydraulic heterogeneity by multiple pumping tests, *Water Resour. Res.*, *43*, W04433, doi:10.1029/2006WR005333.

Linde, N., A. Binley, A. Tryggvason, L. Pedersen, and A. Revil (2006), Improved hydrogeophysical characterization using joint inversion of cross-hole electrical resistance and ground-penetrating radar traveltime data, *Water Resour. Res.*, *42*, W12404, doi:10.1029/2006WR005131.

Linde, N., A. Tryggvason, J. Peterson, and S. Hubbard (2008), Joint inversion of crosshole radar and seismic traveltimes acquired at the South Oyster Bacterial Transport Site, *Geophysics*, *73*, G29.

Liu, X., W. Illman, A. Craig, J. Zhu, and T.-C. J. Yeh (2007), Laboratory sandbox validation of transient hydraulic tomography, *Water Resour. Res.*, *43*, W05404, doi:10.1029/2006WR005144.

Mackay, D., D. Freyberg, P. Roberts, and J. Cherry (1986), A natural gradient experiment on solute transport in a sand aquifer, 1. Approach and overview of plume movement, *Water Resour. Res.*, *22*, 2017–2029.

Malama, B., and B. Johnson (2010), Analytical modeling of saturated zone head response to evapotranspiration and river-stage fluctuations, *J. Hydrol.*, *382*, 1–9.

Molz, F., G. Boman, S. Young, and W. Waldrop (1994), Borehole flowmeters: Field application and data analysis, *J. Hydrol.*, *163*, 347–371.

Moret, G. J. M., W. P. Clement, M. D. Knoll, and W. Barrash (2004), VSP traveltime inversion: Near-surface issues, *Geophysics*, *69*, 345–351.

Moret, G. J. M., M. D. Knoll, W. Barrash, and W. P. Clement (2006), Investigating the stratigraphy of an alluvial aquifer using crosswell seismic traveltime tomography, *Geophysics*, *71*, 63–73.

Morin, R., D. LeBlanc, and W. Teasdale (1988), A statistical evaluation of formation disturbance produced by well-casing installation methods, *Ground Water*, *26*, 207–217.

Mwenifumbo, C., W. Barrash, and M. Knoll (2009), Capacitive conductivity logging and electrical stratigraphy in a high-resistivity aquifer, Boise Hydrogeophysical Research Site, *Geophysics*, *74*, 125.

National Research Council (2000a), *Research Needs in Subsurface Science*, Natl. Acad. Press, Washington, D.C.

National Research Council (2000b), *Seeing into the Earth - Noninvasive Characterization of the Shallow Subsurface for Environmental and Engineering Application*, Natl. Acad. Press, Washington, D.C.

Nyquist, J., P. Freyer, and L. Toran (2008), Stream bottom resistivity tomography to map ground water discharge, *Ground Water*, *46*, 561–569.

Page, J. W. E., K. Soga, and T. Illangasekare (2007), The significance of heterogeneity on mass flux from DNAPL source zones: An experimental investigation, *J. Contam. Hydrol.*, *94*, 215–234.

Paillet, F. L. (1998), Flow modeling and permeability estimation using borehole flow logs in heterogeneous fractured formations, *Water Resour. Res.*, *34*, 997–1010.

Pianosi, J., and D. Belshaw (1990), The Waterloo multilevel groundwater monitoring system, in *8th National Conference on Hazardous Wastes and Hazardous Materials*, pp. 54–57, Hazard. Mater. Control Res. Inst., St. Louis, Mo.

Ptak, T., and G. Schmid (1996), Dual-tracer transport experiments in a physically and chemically heterogeneous porous aquifer: Effective transport parameters and spatial variability, *J. Hydrol.*, *183*, 117–138.

Roberts, P., M. Goltz, and D. Mackay (1986), A natural gradient experiment on solute transport in a sand aquifer: 3. Retardation estimates and mass balances for organic solutes, *Water Resour. Res.*, *22*, 2047–2058.

Singha, K., and S. M. Gorelick (2005), Saline tracer visualized with three-dimensional electrical resistivity tomography: Field-scale spatial moment analysis, *Water Resour. Res.*, *41*, W05023, doi:10.1029/2004WR003460.

Slater, L. (2007), Near surface electrical characterization of hydraulic conductivity: From petrophysical properties to aquifer geometries—A review, *Surv. Geophys.*, *28*, 169–197.

Slater, L., A. Binley, W. Daily, and R. Johnson (2000), Cross-hole electrical imaging of a controlled saline tracer injection, *J. Appl. Geophys.*, *44*, 85–102.

Slater, L., A. Binley, W. Barrash, J. Keery, J. Montrey, and M. Cardiff (2011), An investigation of the ability of induced polarization to resolve aquifer heterogeneity in an unconsolidated sedimentary aquifer, presented at SAGEEP 2011, Environ. and Eng. Geophys. Soc., Charleston, S. C.

Solomon, D., R. Poreda, S. Schiff, and J. Cherry (1992), Tritium and helium: 3 as groundwater age tracers in the Borden aquifer, *Water Resour. Res.*, *28*, 741–755.

Springer, R. K., and L. W. Gelhar (1991), Characterization of large-scale aquifer heterogeneity in glacial outwash by analysis of slug tests with oscillatory response, Cape Cod, Massachusetts, *U.S. Geol. Surv. Tech. Rep., 91-4034*.

Straface, S., T.-C. J. Yeh, J. Zhu, S. Troisi, and C. H. Lee (2007), Sequential aquifer tests at a well field, Montalto Uffugo Scalo, Italy, *Water Resour. Res.*, *43*, W07432, doi:10.1029/2006WR005287.

Straface, S., F. Chidichimo, E. Rizzo, M. Riva, W. Barrash, A. Revil, M. Cardiff, and A. Guadagnini (2011), Joint inversion of steady-state hydrologic and self-potential data for 3D hydraulic conductivity distribution at the Boise Hydrogeophysical Research Site, *J. Hydrol.*, *407*, 115–128, doi:10.1016/j.jhydrol.2011.07.013.

Sudicky, E. (1986), A natural gradient experiment on solute transport in a sand aquifer: Spatial variability of hydraulic conductivity and its role in the dispersion process, *Water Resour. Res.*, *22*, 2069–2082.

Sutton, D. J., Z. J. Kabala, D. E. Schaad, and N. C. Ruud (2000), The dipole-flow test with a tracer: a new single-borehole tracer test for aquifer characterization, *J. Contam. Hydrol.*, *44*, 71–101.

Therrien, R., R. McLaren, E. Sudicky, and S. Panday (2005), Hydrogeosphere: A three-dimensional numerical model describing fully integrated subsurface and surface flow and solute transport, technical report, Univ. of Waterloo, Waterloo, Ontario, Canada.

Tronicke, J., K. Holliger, W. Barrash, and M. D. Knoll (2004), Multivariate analysis of cross-hole georadar velocity and attenuation tomograms for aquifer zonation, *Water Resour. Res.*, *40*, W01519, doi:10.1029/2003WR002031.

Vasco, D. (2008), Zeroth-order inversion of transient pressure observations, *Inv. Probl.*, *24*, 513.

Vasco, D., and K. Karasaki (2001), Inversion of pressure observations: an integral formulation, *J. Hydrol.*, *253*, 27–40.

Vasco, D., and K. Karasaki (2006), Interpretation and inversion of low-frequency head observations, *Water Resour. Res.*, *42*, W05408, doi:10.1029/2005WR004445

Vasco, D., H. Keers, and K. Karasaki (2000), Estimation of reservoir properties using transient pressure data: An asymptotic approach, *Water Resour. Res.*, *36*, 3447–3465.

Watson, D. B., W. E. Doll, T. J. Gamey, J. R. Sheehan, and P. M. Jardine (2005), Plume and lithologic profiling with surface resistivity and seismic tomography, *Ground Water*, *43*, 169–177.

Weissmann, G., Y. Zhang, E. LaBolle, and G. Fogg (2002), Dispersion of groundwater age in an alluvial aquifer system, *Water Resour. Res.*, *38*(10), 1198, doi:10.1029/2001WR000907.

Williams, J., and F. Paillet (2002), Using flowmeter pulse tests to define hydraulic connections in the subsurface: A fractured shale example, *J. Hydrol.*, *265*, 100–117.

Wu, C.-M., T.-C. J. Yeh, J. Zhu, T. H. Lee, N.-S. Hsu, C.-H. Chen, and A. F. Sancho (2005), Traditional analysis of aquifer tests: Comparing apples to oranges?, *Water Resour. Res.*, *41*, W09402, doi:10.1029/2004WR003717.

Yeh, T., J. Xiang, R. Suribhatla, K. Hsu, C. Lee, and J. Wen (2009), River stage tomography: A new approach for characterizing groundwater basins, *Water Resour. Res.*, *45*, W05409, doi:10.1029/2008WR007233.

Zhu, J., and J. T.-C. Yeh (2005), Characterization of aquifer heterogeneity using transient hydraulic tomography, *Water Resour. Res.*, *41*, W07028, doi:10.1029/2004WR003790.

Zlotnik, V. A., and V. L. McGuire (1998), Multi-level slug tests in highly permeable formations: 1. modification of the Springer-Gelhar (SG) model, *J. Hydrol.*, *204*, 271–282.

Zlotnik, V., and B. Zurbuchen (1998), Dipole probe: Design and field applications of a single borehole device for measurements of vertical variations of hydraulic conductivity, *Ground Water*, *36*, 884–893.

W. Barrash, Department of Geosciences, Center for Geophysical Investigation of the Shallow Subsurface, Boise State University, 1910 University Dr., Boise, ID 83705-1535, USA. (wbarrash@cgiss.boisestate.edu)

M. Cardiff, Department of Geoscience, University of Wisconsin-Madison, Weeks Hall, 1215 W. Dayton St., Madison, WI 53706, USA. (cardiff@wisc.edu)

P. K. Kitanidis, Department of Civil and Environmental Engineering, Stanford University, Yang and Yamazaki Environment and Energy Bldg., MC 4020, 473 Via Ortega, Stanford, CA 94305, USA. (peterk@stanford.edu)